proliferation (Fig. 4B, c and d). Collectively these results are consistent with the hypothesis that increased FGF production by the *Hand2*-null uterine stroma stimulates epithelial proliferation by activating the FGFR-ERK1/2 pathway.

The ERK1/2-dependent phosphorylation of epithelial ERα at Ser^{118} is critical for the transcriptional activation of ERα (*11*). Administration of either PD173074 (Fig. 4C, a to d) or PD184352 (Fig. 4C, e to h) to *Hand2*-null uterine horns blocked the phosphorylation of epithelial ERα at Ser^{118} and the expression of Muc-1. This result supported our view that elevated signaling by FGFR-ERK1/2 pathway in $Hand2^{d/d}$ uteri is responsible for phosphorylation and activation of ERα in epithelial cells, which promotes persistent expression of Muc-1 and which in turn creates a barrier that prevents embryo attachment.

Earlier studies using tissue recombinants prepared with uterine epithelium and stroma isolated from neonatal wild-type and PR-null mice indicated that the stromal PR plays an obligatory role in mediating the inhibitory actions of P on E-induced epithelial cell proliferation (*18*). However, the mechanism of this stromal-epithelial communication remained unknown. Our study has delineated a pathway in which Hand2 operates downstream of P to regulate the production of FGFs, mitogenic paracrine signals that originate in the stroma and act on the FGFR(s) in epithelium to control its E responsiveness (fig. S15). The antiproliferative action of P in uterine epithelium is of clinical significance, because the breakdown of this action underpins E-dependent endometrial cancer (*19*). Hand2, therefore, is an important factor to be considered for hormone therapy to block the proliferative actions of E in the endometrium.

References and Notes

1. C. A. Finn, L. Martin, *J. Reprod. Fertil.* **39**, 195 (1974).
2. D. D. Carson *et al.*, *Dev. Biol.* **223**, 217 (2000).
3. C. Y. Ramathal, I. C. Bagchi, R. N. Taylor, M. K. Bagchi, *Semin. Reprod. Med.* **28**, 17 (2010).
4. L. Martin, R. M. Das, C. A. Finn, *J. Endocrinol.* **57**, 549 (1973).
5. I. C. Bagchi, Y. P. Cheon, Q. Li, M. K. Bagchi, *Front. Biosci.* **8**, s852 (2003).
6. H. Pan, Y. Deng, J. W. Pollard, *Proc. Natl. Acad. Sci. U.S.A.* **103**, 14021 (2006).
7. I. C. Bagchi *et al.*, *Semin. Reprod. Med.* **23**, 38 (2005).
8. D. Srivastava *et al.*, *Nat. Genet.* **16**, 154 (1997).
9. A. B. Firulli, *Gene* **312**, 27 (2003).
10. Materials and methods are available as supporting material on *Science* Online.
11. S. Kato *et al.*, *Science* **270**, 1491 (1995).
12. G. A. Surveyor *et al.*, *Endocrinology* **136**, 3639 (1995).
13. K. Y. Lee *et al.*, *Nat. Genet.* **38**, 1204 (2006).
14. V. P. Eswarakumar, I. Lax, J. Schlessinger, *Cytokine Growth Factor Rev.* **16**, 139 (2005).
15. R. Iwamoto, E. Mekada, *Cytokine Growth Factor Rev.* **11**, 335 (2000).
16. M. Koziczak, T. Holbro, N. E. Hynes, *Oncogene* **23**, 3501 (2004).
17. D. B. Solit *et al.*, *Nature* **439**, 358 (2006).
18. T. Kurita *et al.*, *Endocrinology* **139**, 4708 (1998).
19. J. J. Kim, E. Chapman-Davis, *Semin. Reprod. Med.* **28**, 81 (2010).

20. We thank M. Laws for genotyping and Y. Li for immunohistochemistry. This work was supported by the Eunice Kennedy Shriver National Institute of Child Health and Human Development, NIH, through U54HD055787 as part of the Specialized Cooperative Centers Program in Reproduction and Infertility Research. The Gene Expression Omnibus (GEO) microarray accession number is GSE25881.

Supporting Online Material

www.sciencemag.org/cgi/content/full/331/6019/912/DC1
Materials and Methods
Figs. S1 to S15
Table S1
References

7 September 2010; accepted 15 December 2010
10.1126/science.1197454

Distinct Properties of the XY Pseudoautosomal Region Crucial for Male Meiosis

Liisa Kauppi,[1] Marco Barchi,[2,3] Frédéric Baudat,[2]* Peter J. Romanienko,[2] Scott Keeney,[1,4]† Maria Jasin[2]†

Meiosis requires that each chromosome find its homologous partner and undergo at least one crossover. X-Y chromosome segregation hinges on efficient crossing-over in a very small region of homology, the pseudoautosomal region (PAR). We find that mouse PAR DNA occupies unusually long chromosome axes, potentially as shorter chromatin loops, predicted to promote double-strand break (DSB) formation. Most PARs show delayed appearance of RAD51/DMC1 foci, which mark DSB ends, and all PARs undergo delayed DSB-mediated homologous pairing. Analysis of *Spo11*β isoform–specific transgenic mice revealed that late RAD51/DMC1 foci in the PAR are genetically distinct from both early PAR foci and global foci and that late PAR foci promote efficient X-Y pairing, recombination, and male fertility. Our findings uncover specific mechanisms that surmount the unique challenges of X-Y recombination.

Meiotic recombination, initiated by programmed double-strand breaks (DSBs), promotes homologous chromosome (homolog) pairing during prophase I (*1*). A subset of DSBs matures into crossovers that physically connect homologs so that they orient properly on the first meiotic spindle. Because sex chromosome recombination and pairing are restricted to the PAR (*2*), at least one DSB must form within this small region, and the homologous PAR must be located and engaged in recombination to lead to a crossover. Accordingly, the PAR in males exhibits high crossover frequency (*2*, *3*), but sex chromosomes also missegregate more frequently than autosomes (*4*). Nevertheless, X-Y nondisjunction is rare, which suggests that there are mechanisms that ensure successful X-Y recombination.

X-Y pairing is more challenging than autosomal pairing, as it cannot be mediated by multiple DNA interactions along the length of the chromosomes. We used fluorescence in situ hybridization (FISH) (*5*) to compare timing of meiotic X-Y and autosomal pairing in mice (Fig. 1). At leptonema, when DSBs begin to form and only short chromosome axis segments are present, PAR and autosomal FISH probes were mostly unpaired. By early to mid-zygonema, when axes elongate and homologs become juxtaposed, distal ends of chr 18 and 19 were paired in ~50% of nuclei; by late zygonema, these regions were paired in nearly all nuclei (Fig. 1B and fig. S1). In contrast, the X and Y PARs were rarely paired before pachynema (Fig. 1B); hence, X-Y pairing is delayed compared with that of autosomes.

DSBs precede and are required for efficient homolog pairing in mouse meiosis (*6*, *7*). Nucleus-wide ("global") foci of DSB markers RAD51/DMC1 peak in number at early to mid-zygonema (Fig. 2A) (*8*, *9*). Because stable X-Y pairing occurs late, we asked whether PAR DSB kinetics is also delayed (Fig. 2B and fig. S2). More than half of cells had no RAD51/DMC1 focus in the PAR before late zygonema (Fig. 2C), distinct from global patterns. Only when global foci were already declining did the majority of cells (~70%) display PAR foci (Fig. 2C and fig. S2*i*). We interpret the lack of PAR foci to indicate that DSBs have not yet formed. Thus, we propose that PAR DSB formation and/or turnover are under distinct temporal control. We cannot exclude the alternative possibility that PAR DSBs have formed but are cytologically undetectable, for example, because RAD51/DMC1 have not yet been loaded onto DSB ends or because foci have already turned over. In either case, DSB dynamics and/or processing differs on the PAR.

Most sites marked by PAR RAD51/DMC1 foci appeared incapable of mediating stable pairing before early pachynema (~70% of late zygotene

[1]Molecular Biology Program, Memorial Sloan-Kettering Cancer Center, New York, NY 10065, USA. [2]Developmental Biology Program, Memorial Sloan-Kettering Cancer Center, New York, NY 10065, USA. [3]Department of Public Health and Cell Biology, Section of Anatomy, University of Rome Tor Vergata, 00133 Rome, Italy. [4]Howard Hughes Medical Institute, Memorial Sloan-Kettering Cancer Center, New York, NY 10065, USA.

*Present address: Institute of Human Genetics, CNRS, 34090 Montpellier, France.

†To whom correspondence should be addressed. E-mail: m-jasin@ski.mskcc.org (M.J.); s-keeney@ski.mskcc.org (S.K.)

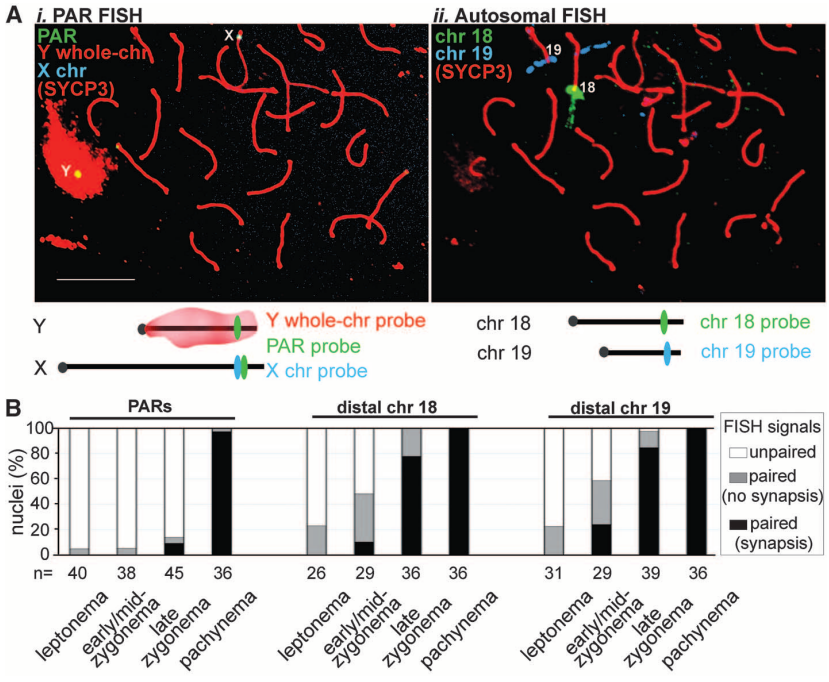

Fig. 1. Late PAR pairing during male meiosis. (**A**) FISH assay for pairing. (*i* and *ii*) Example of immunofluorescence (IF) and two sequential rounds of FISH on a late zygotene spermatocyte nucleus. Nuclei stained with an antibody against axis protein SYCP3 were subjected first to PAR FISH (*i*), then to distal chr 18 and distal chr 19 FISH (*ii*). Scale bar, 10 μm. (**B**) Nuclei (%) with unpaired and paired (≤2 μm apart) FISH signals. Chromosome synapsis status was also recorded at sites of paired signals.

nuclei had foci, but <20% showed PAR pairing) (Figs. 1B and 2C). The number of PAR foci per cell also increased over time. In leptonema and early to mid-zygonema, most cells with a PAR RAD51/DMC1 focus had only one (typically on X), whereas by late zygonema, two PAR foci were often present (both X and Y) (Fig. 2C). Foci on both PARs could represent two independent DSBs. If so, then having more than one X-Y recombination interaction may stabilize pairing, similar to multiple interactions that stabilize pairing of autosomes (*10*). Alternatively, foci on both PARs could represent the two, separated ends of a single DSB (*11*, *12*)—with one focus marking the broken PAR and the second focus marking the other PAR (fig. S3A). In this "ends-apart" model, nuclei that have two PAR foci are those in which the X and Y PARs have successfully engaged each other. However, we found that most such nuclei showed no evidence of a preferential X-Y spatial relationship (fig. S3B), and most PAR pairing occurred abruptly at the zygonema-to-pachynema transition, i.e., after the stage when many cells displayed two PAR foci (compare Figs. 1B and 2C). Sex body formation (*13*) may facilitate this sudden completion of X-Y pairing by providing homology-independent X-Y proximity that simplifies the homology search.

The haploid mouse genome averages fewer than one DSB per 10 Mb (Fig. 2A), whereas the

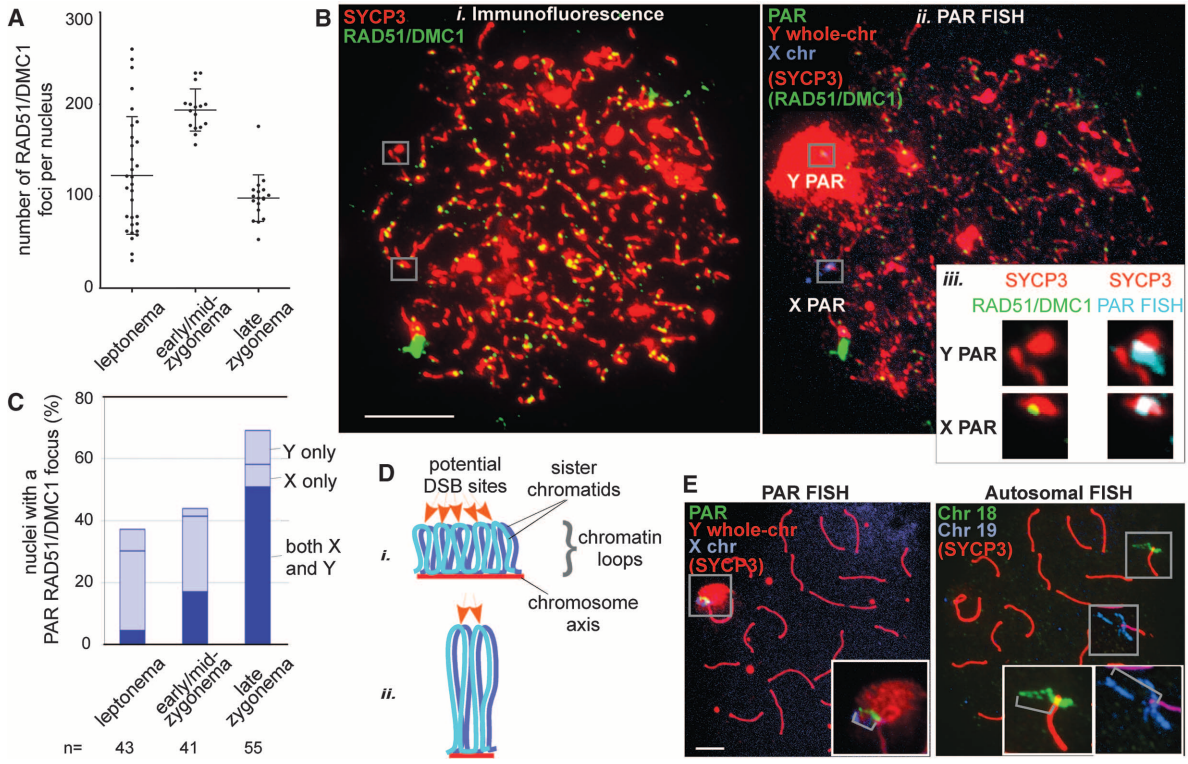

Fig. 2. Distinct temporal and structural properties of the PAR. (**A**) Nucleus-wide RAD51/DMC1 foci in spermatocytes (bars show means ± SD). (**B**) Assay for PAR DSB formation. IF against RAD51/DMC1 and SYCP3 (*i*) and FISH (*ii*) with probes shown in Fig. 1A*i* on a leptotene spermatocyte nucleus. Scale bar, 10 μm. (*iii*) Magnified views of Y and X PARs from frames in (*i*) (*5*) and an overlay of the PAR FISH signal with SYCP3 (right), here with a RAD51/DMC1 focus only on the X PAR. (**C**) Nuclei (%) with one or two PAR RAD51/DMC1 foci. (**D**) Axis/loop segments as a determinant of DSB potential [after (*15*)]. Only one homolog is shown. DNA organized on a longer axis into more and smaller loops (*i*) has more DSB potential than if the same DNA is organized on a shorter axis into fewer and larger loops (*ii*). (**E**) Examples of chromatin extension (gray brackets in insets); see also Table 1. Scale bar, 5 μm.

<1 Mb PAR (*14*) undergoes one or two DSBs (Fig. 2C), which is 10 to 20 times the genome average. We speculated that distinct higher-order chromosome structure could render the PAR more conducive to DSB formation. Meiotic recombination is proposed to occur within DNA segments residing in chromatin loops that become transiently tethered to chromosome axes (*15*). Loop density per micrometer of axis is constant (*16*) and produces an inverse relation between loop size and axis length (*17*). DNA arranged into smaller loops may have higher DSB potential (Fig. 2D) (*18*); indeed, autosomal crossover frequency in male mice correlates with axis length (*19*). We found that PAR axes were disproportionately long relative to DNA length and incorporated ~1 Mb per μm of axis (Table 1A). At the distal ends of chr 18 and 19 (regions with relatively frequent crossing-over) (*19*), DNA content was 10 to 13 Mb per μm and correlated well with axis length, i.e., the distal ~10% of DNA occupied ~10% total axis length (Table 1A). The ≥10-fold difference between PAR and autosome axes is of the magnitude expected for a region that experiences more than 10 times as many DSBs. Axes of non-PAR portions of the X and Y had a DNA content more like autosomes (≥14 Mb per μm) (fig. S4).

Long PAR axes predict short chromatin loops. As a proxy for loop size, we measured FISH signal extension from axes for probes in the PAR and autosomal subtelomeric regions (Fig. 2E and Table 1B). PAR FISH signals were substantially more compact at all stages (about one-third to one-seventh as extended), consistent with smaller loops. Thus, chromosome structure could be one factor that facilitates high-frequency DSB formation in the PAR.

The distinct temporal and structural features outlined above raised the possibility that mechanisms ensuring efficient PAR recombination and pairing may be under different genetic control from autosomes. Characterization of a variant of SPO11, the evolutionarily conserved meiotic DSB catalyst (*1*), validated this hypothesis (Fig. 3). Two major mRNA splicing isoforms in mice and humans are *Spo11*α and *Spo11*β (*7*, *20*–*22*) (Fig. 3A*i* and fig. S5). *Spo11*β is expressed early in meiosis, when most DSBs are formed, whereas *Spo11*α is expressed later (*7*, *20*, *23*) (Fig. 3A*ii* and fig. S6A). Thus, SPO11β is likely responsible for most DSB formation.

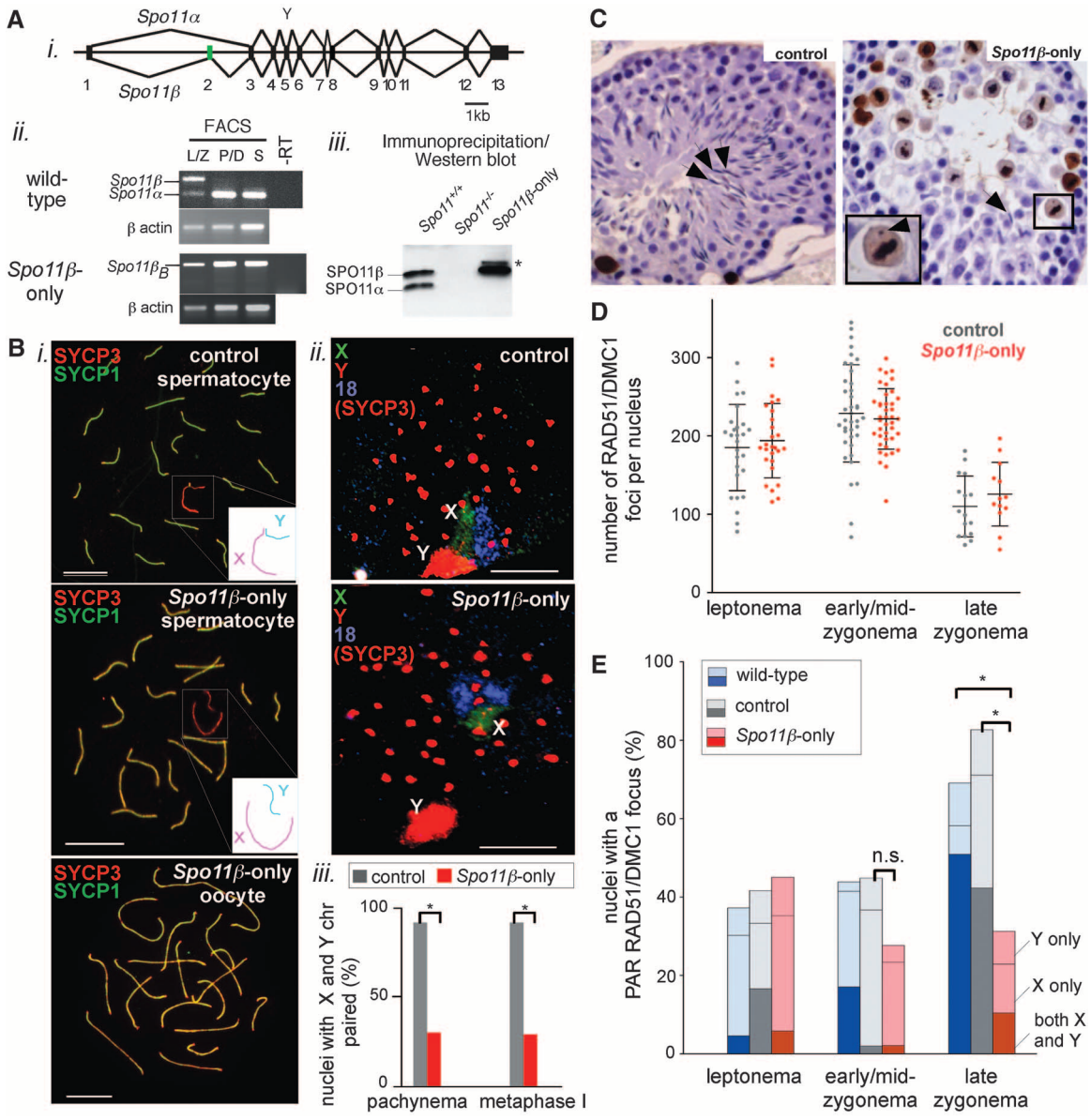

Fig. 3. Genetic control of PAR recombination and pairing. (**A**) *Spo11* splice variants (see also fig. S5). (*i*) Genomic organization and splicing. *Spo11*β includes exon 2, *Spo11*α excludes it. Y, catalytic tyrosine. (*ii* and *iii*) Reverse transcription polymerase chain reaction from flow-sorted meiocyte populations of adult mice. –RT, no reverse transcription; L/Z, leptonema/zygonema; P/D, pachynema/diplonema; S, spermatids. (*iv*) SPO11 protein levels in adult testis extracts. Asterisk, a lower-mobility protein likely originating from the knockout allele (fig. S6D). (**B**) IF of SYCP1 and SYCP3 on pachytene nuclei (*i*) and of SYCP3 plus whole-chromosome FISH of early metaphase I spermatocyte nuclei (*ii*) from mice of the indicated genotypes. Inset in (*i*), schematic of X and Y chromosomes. Scale bars, 10 μm. (*iii*) Quantification of X-Y association; 57 to 65 nuclei scored per genotype. (**C**) Terminal deoxynucleotidyl transferase–mediated deoxyuridine triphosphate nick end labeling (TUNEL)–stained testis sections; apoptotic cells stain brown. Elongating spermatids (arrows) are rare in *Spo11*β-only mice. Inset shows a lagging chromosome (arrowhead) in a TUNEL-positive cell. (**D**) RAD51/DMC1 focus counts in spermatocytes from control and *Spo11*β-only mice (bars show means ± SD). (**E**) Nuclei (%) with PAR RAD51/DMC1 foci in mice of the indicated genotypes; for each genotype, 41 to 55 nuclei were scored per stage. *$P \leq 0.0002$ (two-tailed Mann-Whitney test); n.s., not significant ($P = 0.09$).

Table 1. Chromosome axis lengths and chromatin extension in PARs and distal ends of chr 18 and 19. Axis lengths are means ± SD and FISH signal extensions are means ± SD, for the number of observations in parentheses. Probe size is the size of the bacterial artificial chromosome (*5*).

(**A**) DNA content versus chromosome axis lengths (late zygonema)

Chromosome	Total size (Mb)	Probe-distal region (Mb)	Total chromosome axis (μm)	Probe-distal axis	
				Length (μm)	DNA content (Mb/μm)
Y	95	0.7	4.2 ± 0.7 (17)	0.7 ± 0.2 (20)	1
X	167	0.7	12.7 ± 2.8 (13)	0.8 ± 0.2 (23)	1
18	91	8	6.1 ± 0.9 (11)	0.6 ± 0.1 (12)	13
19	61	6	5.1 ± 0.5 (11)	0.6 ± 0.1 (10)	10

(**B**) Length of chromatin extension from axes

Locus	Probe size (kb)	FISH signal extension (μm)			
		Leptonema	Early to mid-zygonema	Late zygonema	Pachynema
Y PAR	146	0.5 ± 0.2 (25)	0.6 ± 0.3 (21)	0.6 ± 0.3 (21)	1.2 ± 0.5 (23)*
X PAR		0.6 ± 0.4 (23)	0.7 ± 0.5 (17)	0.6 ± 0.5 (20)	
Distal chr 18	207	2.2 ± 0.8 (26)	3.2 ± 1.5 (31)*	4.5 ± 1.9 (35)*	5.4 ± 2.2 (21)*
Distal chr 19	182	2.3 ± 0.9 (18)	3.6 ± 2.0 (33)*	5.3 ± 3.0 (40)*	5.9 ± 2.3 (23)*

*Some or all measurements are from paired FISH signals.

We generated transgenic mice expressing *Spo11*β_B cDNA (fig. S5) from a meiosis-specific promoter (*24*) (fig. S6B). *Tg(Xmr-Spo11*β_B*)* transcript expression overlapped with *Spo11*β mRNA appearance in wild type (Fig. 3A*ii* and fig. S6, A and C). In testis extracts of *Spo11*$^{-/-}$ *Tg(Xmr-Spo11*β_B*)*$^{+/+}$ (hereafter, "*Spo11*β-only") mice, SPO11β_B protein approximated the total level of SPO11 in wild type (Fig. 3A*iii*). The transgene did not cause obvious meiotic phenotypes in mice heterozygous at the endogenous *Spo11* locus [i.e., *Spo11*$^{+/-}$ *Tg(Xmr-Spo11*β_B*)*$^{+/+}$], and these mice were used as controls. The profound meiotic defects of *Spo11*$^{-/-}$ mice [no recombination, failure of homolog pairing and synapsis, and infertility (*6*, *7*, *25*)] were mostly rescued by *Tg(Xmr-Spo11*β_B*)* in both sexes: Autosomal homologous pairing, synapsis, and MLH1 focus formation (a crossover marker) appeared normal (Fig. 3B*i* and fig. S7A). Moreover, ovaries of *Spo11*β-only mice contained abundant primordial follicles (fig. S7B), and *Spo11*β-only females were fully fertile with normal litter sizes. Thus SPO11β_B supports autosomal crossing-over, pairing, and synapsis, and (in females) full meiotic progression and accurate chromosome segregation. Male meiosis was not fully rescued, however. Although sex bodies formed (fig. S7C), the X and Y failed to pair and synapse in ~70% of spermatocytes (Fig. 3B). *Spo11*β-only testis sections showed numerous apoptotic metaphase I cells (Fig. 3C), many with a lagging chromosome (Fig. 3C, inset, and fig. S7D), consistent with spindle checkpoint-induced apoptosis (*9*, *26*, *27*), triggered by the failure of nonrecombinant X and Y to orient properly on the metaphase I spindle. Few postmeiotic cells were formed, and testis sizes were reduced (Fig. 3C and fig. S7, D and E), so that although some *Spo11*β-only males produced offspring, most were infertile.

Nucleus-wide numbers and timing of RAD51/DMC1 foci were indistinguishable between *Spo11*β-only and control males (Fig. 3D and fig. S7F), which indicated that the X-Y pairing defect cannot be attributed to reduced global DSB levels. Similarly, the frequency of PAR RAD51/DMC1 foci in leptonema was not affected (Fig. 3E). In contrast, the percentage of late zygotene nuclei with a PAR focus was reduced in *Spo11*β-only males, consistent with a defect in a late-forming DSB population (PAR-specific, or possibly including a small subset of autosomal DSBs). About 70% of late zygotene nuclei lacked PAR foci (Fig. 3E), which was similar to the percentage of cells with X-Y pairing failure (Fig. 3B*iii*). Thus, the few PAR foci that form early in both wild-type and *Spo11*β-only males seem to persist until late zygonema (fig. S4, discussion), at which time recombination-mediated X-Y pairing occurs. We propose that a lack of late PAR DSBs is the cause of infertility in *Spo11*β-only males. In females, two fully homologous X chromosomes make PAR recombination dispensable.

*Spo11*α is the only splice variant missing from *Spo11*β-only mice that is known to be developmentally regulated, and its expression in wild type correlates with the timing of late PAR DSBs as inferred from the appearance of RAD51/DMC1 foci. It is thus possible that SPO11α, by itself or in combination with SPO11β, is needed for DSB formation in late zygonema. In this scenario, late-forming PAR DSBs are genetically separable from both global DSBs and early-forming PAR DSBs, and the surge of late-forming PAR DSBs is crucial for efficient X-Y pairing and fertility. PAR recombination occasionally fails in humans, as evidenced by paternally inherited sex chromosome aneuploidies [e.g., Klinefelter's or Turner syndromes (*28*)]. Because *Spo11* isoforms are conserved, we speculate that variation in *Spo11* splicing patterns may be a human X-Y nondisjunction susceptibility trait.

References and Notes

1. F. Cole, S. Keeney, M. Jasin, *Genes Dev.* **24**, 1201 (2010).
2. F. Rouyer *et al.*, *Nature* **319**, 291 (1986).
3. P. Soriano *et al.*, *Proc. Natl. Acad. Sci. U.S.A.* **84**, 7218 (1987).
4. Q. Shi *et al.*, *Am. J. Med. Genet.* **99**, 34 (2001).
5. Materials and methods are available as supporting material on *Science* Online.
6. F. Baudat, K. Manova, J. P. Yuen, M. Jasin, S. Keeney, *Mol. Cell* **6**, 989 (2000).
7. P. J. Romanienko, R. D. Camerini-Otero, *Mol. Cell* **6**, 975 (2000).
8. X. Ding *et al.*, *Dev. Cell* **12**, 863 (2007).
9. M. Barchi *et al.*, *PLoS Genet.* **4**, e1000076 (2008).
10. B. M. Weiner, N. Kleckner, *Cell* **77**, 977 (1994).
11. N. Hunter, in *Molecular Genetics of Recombination*, A. Aguilera, Rothstein, R., Eds. (Springer-Verlag, Heidelberg, 2007), vol. 17, pp. 381–442.
12. A. Storlazzi *et al.*, *Cell* **141**, 94 (2010).
13. P. S. Burgoyne, S. K. Mahadevaiah, J. M. Turner, *Nat. Rev. Genet.* **10**, 207 (2009).
14. J. Perry, S. Palmer, A. Gabriel, A. Ashworth, *Genome Res.* **11**, 1826 (2001).
15. Y. Blat, R. U. Protacio, N. Hunter, N. Kleckner, *Cell* **111**, 791 (2002).
16. D. Zickler, N. Kleckner, *Annu. Rev. Genet.* **33**, 603 (1999).
17. E. Revenkova *et al.*, *Nat. Cell Biol.* **6**, 555 (2004).
18. N. Kleckner, A. Storlazzi, D. Zickler, *Trends Genet.* **19**, 623 (2003).
19. L. Froenicke, L. K. Anderson, J. Wienberg, T. Ashley, *Am. J. Hum. Genet.* **71**, 1353 (2002).
20. P. J. Romanienko, R. D. Camerini-Otero, *Genomics* **61**, 156 (1999).
21. S. Keeney *et al.*, *Genomics* **61**, 170 (1999).
22. M. A. Bellani, K. A. Boateng, D. McLeod, R. D. Camerini-Otero, *Mol. Cell. Biol.* **30**, 4391 (2010).
23. M. J. Neale, J. Pan, S. Keeney, *Nature* **436**, 1053 (2005).
24. P. J. Romanienko, dissertation, Cornell University Ithaca, NY (1997).
25. M. Di Giacomo *et al.*, *Proc. Natl. Acad. Sci. U.S.A.* **102**, 737 (2005).
26. S. Eaker, J. Cobb, A. Pyle, M. A. Handel, *Dev. Biol.* **249**, 85 (2002).

27. T. Odorisio, T. A. Rodriguez, E. P. Evans, A. R. Clarke, P. S. Burgoyne, *Nat. Genet.* **18**, 257 (1998).
28. H. Hall, P. Hunt, T. Hassold, *Curr. Opin. Genet. Dev.* **16**, 323 (2006).
29. This work was supported by NIH grant R01 HD040916 (M.J. and S.K); International Grants in Cancer Research (AIRC) [My First AIRC Grant (MFAG) grant 4765], Italian Ministry for Education, University and Research (MIUR), the Lalor Foundation, and the American-Italian Cancer Foundation (AICF) (M.B.); and the Charles H. Revson Foundation (F.B.). We thank M. Leversha [Memorial Sloan-Kettering Cancer Center (MSKCC)], P. Bois (Scripps Florida), and K. Manova (MSKCC) for valuable advice and protocols. We are grateful to Keeney and Jasin lab members, especially I. Roig, E. de Boer, and F. Cole, and to N. Hunter (University of California, Davis) for insightful comments.

Supporting Online Material
www.sciencemag.org/cgi/content/full/331/6019/916/DC1
SOM Text
Materials and Methods
Figs. S1 to S7
References

28 July 2010; accepted 21 December 2010
10.1126/science.1195774

Classic Selective Sweeps Were Rare in Recent Human Evolution

Ryan D. Hernandez,[1]* Joanna L. Kelley,[1] Eyal Elyashiv,[2] S. Cord Melton,[1] Adam Auton,[3] Gilean McVean,[3,4] 1000 Genomes Project, Guy Sella,[2]† Molly Przeworski[1,5,6]†‡

Efforts to identify the genetic basis of human adaptations from polymorphism data have sought footprints of "classic selective sweeps" (in which a beneficial mutation arises and rapidly fixes in the population). Yet it remains unknown whether this form of natural selection was common in our evolution. We examined the evidence for classic sweeps in resequencing data from 179 human genomes. As expected under a recurrent-sweep model, we found that diversity levels decrease near exons and conserved noncoding regions. In contrast to expectation, however, the trough in diversity around human-specific amino acid substitutions is no more pronounced than around synonymous substitutions. Moreover, relative to the genome background, amino acid and putative regulatory sites are not significantly enriched in alleles that are highly differentiated between populations. These findings indicate that classic sweeps were not a dominant mode of human adaptation over the past ~250,000 years.

Humans have experienced myriad adaptations since the common ancestor with chimpanzees and more recently have adapted to a wide range of environments. Efforts to infer the molecular basis of these adaptations from polymorphism data have largely been guided by the "classic selective sweep" model, in which a new, strongly beneficial mutation increases in frequency to fixation in the population [reviewed in (*1*, *2*)]. In this scenario, the allele ascends rapidly enough in frequency for there to be little opportunity for recombination to uncouple it from its genetic background, such that its rise sweeps out variation at linked sites, reducing linked neutral diversity in the population and distorting allele frequencies and patterns of linkage disequilibrium (*3*). In humans, the effects of sweeps are expected to persist for approximately 10,000 generations or about 250,000 years (*4*).

Identifying the footprint of a sweep against a noisy genomic background is challenging, because patterns of genetic variation reflect the effects of multiple modes of natural selection as well as of demographic history, mutation, and recombination. To date, applications of statistical tests based on the sweep model have led to the identification of more than 2000 genes as potential targets of positive selection in the human genome (*2*) and to the suggestion that diversity patterns in ~10% of the human genome have been affected by linkage to recent sweeps [e.g., (*5*)]. The list of functionally characterized cases of genetic adaptations is short, however, and the false discovery rate of selection scans is potentially high (*6*). Thus, it remains unknown whether the well-documented cases are typical of human adaptations, or whether they represent rare instances where the genetic architecture of the adaptation was conducive to classic sweeps (*7*, *8*), with most adaptations occurring by other modes (e.g., polygenic selection and selection on standing variation).

Two main lines of evidence have been advanced in support of the hypothesis that classic selective sweeps were common. First, regions of low recombination, in which a single sweep should have a larger span, exhibit lower diversity (after correcting for variation in mutation rates) relative to regions of high recombination (*9*–*11*). Regions of low recombination also show greater differentiation between populations (*12*), as expected from local adaptation or, for some parameters, from the fixation of globally advantageous alleles (*13*). Second, under the sensible assumption that amino acid and conserved noncoding sites are enriched among targets of adaptation, one would expect that the signal of selection would be most clearly visible at or around such sites [e.g., (*10*, *14*)]. Consistent with this expectation, diversity levels decrease with the number of human-specific substitutions at amino acid or conserved noncoding sites (in 200- to 600-kb windows) (*10*), and genic regions show an enrichment of alleles that are highly differentiated between populations relative to nongenic regions (*15*, *16*). These patterns are informative but are only indirectly related to theoretical predictions. Moreover, some—possibly all—of these patterns may instead result from purifying selection acting on deleterious mutations at linked sites ("background selection") (*9*–*11*, *16*–*18*).

To evaluate the importance of classic sweeps in shaping human diversity, we analyzed resequencing data for 179 human genomes from four populations, collected as part of the low-coverage pilot for the 1000 Genomes Project (*19*). These data overcome ascertainment biases arising in the study of genotyping data, with ~99% power to detect variants with a population frequency above 10% for 86% of the euchromatic genome (*19*).

We examined the extent to which selection affects diversity levels at linked sites by calculating the average diversity as a function of genetic distance from the nearest exons, collating all exons across the genome (fig. S1). To estimate neutral diversity levels, we focused only on nonconserved noncoding and fourfold degenerate sites (*11*). To correct for systematic variation in the mutation rate, we divided diversity by human–rhesus macaque divergence [to which the contribution of ancestral polymorphism is minor (*11*)]. Our estimate of relative diversity appears little affected by the low fold coverage of individuals or variation in sequencing depth (fig. S2, C to E). Scaled diversity levels are lowest near exons (Fig. 1A and fig. S3), recovering half the drop by 0.03 to 0.04 cM, depending on the population, and 80% by 0.07 to 0.1 cM [see (*20*)]. Given that diversity is scaled by divergence, the trough in scaled diversity around exons does not reflect systematic variation in mutation rates as a function of the distance from exons, strong purifying selection on the sites themselves (which would decrease both diversity and divergence), or weak selection near exons (which should inflate, not decrease, diversity levels divided by divergence). Rather, the trough provides evidence for the effects of directional selection at linked sites, extending over 100 kb.

[1]Department of Human Genetics, University of Chicago, Chicago, IL 60637, USA. [2]Department of Ecology, Evolution and Behavior, Hebrew University of Jerusalem, Givat Ram, Jerusalem 91904, Israel. [3]Wellcome Trust Centre for Human Genetics, University of Oxford, Oxford OX3 7BN, UK. [4]Department of Statistics, University of Oxford, Oxford OX1 3TG, UK. [5]Department of Ecology and Evolution, University of Chicago, Chicago, IL 60637, USA. [6]Howard Hughes Medical Institute, University of Chicago, Chicago, IL 60637, USA.

*Present address: Department of Bioengineering and Therapeutic Sciences, University of California, San Francisco, CA 94143, USA.
†These authors contributed equally to this work.
‡To whom correspondence should be addressed. E-mail: mfp@uchicago.edu